GEOARCHAEOLOGICAL XRF LAB

GEOARCHAEOLOGICAL X-RAY FLUORESCENCE SPECTROMETRY LABORATORY
8100 WYOMING BLVD., SUITE M4-158 ALBUQUERQUE, NM 87113 USA

ENERGY-DISPERSIVE X-RAY FLUORESCENCE (EDXRF) ANALYSIS OF MAJOR AND MINOR OXIDE AND TRACE ELEMENT CONCENTRATIONS FOR IRON OXIDE (OCHRE) SAMPLES FROM THREE MINE LOCATIONS AND THE BEACH PALEOINDIAN CACHE IN NORTH DAKOTA

DRAFT

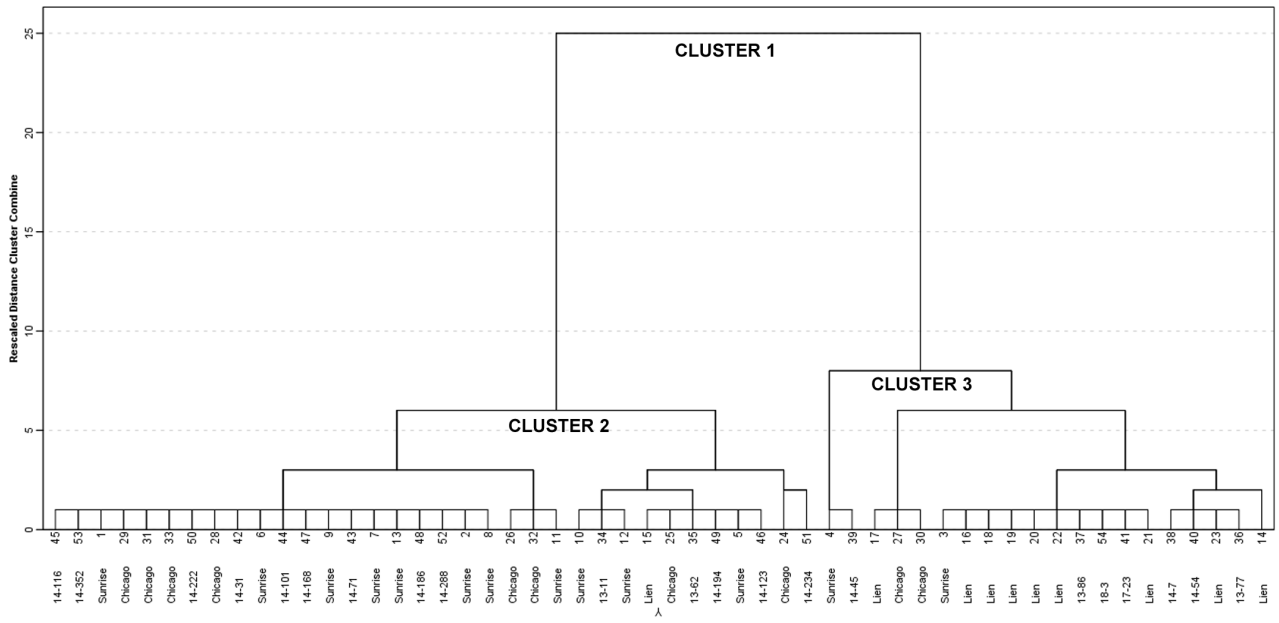

by

M. Steven Shackley Ph.D., Director
Geoarchaeological XRF Laboratory
Albuquerque, New Mexico

Report Prepared for

Dr. Bruce Huckell
Department of Anthropology
University of New Mexico, Albuquerque

11 July 2021

INTRODUCTION

The non-destructive whole rock EDXRF analysis here of source standards from the Lien Sunrise and Chicago iron mines and the Beach Paleoindian Cache in North Dakota indicate a good statistical correlation between the source rocks and the archaeological ochre (hematite) from the cache. An analytical trajectory of parametric and non-parametric multivariate and graphical statistical procedures was employed to determine source provenance (see Baxter 1994; Johnson and Wichern 1998; Shennan 1997; c.f. Zarzycka et al. 2019).

The presence of red ochre, a ferrous iron oxide (Fe_2O_3) in North American Paleoindian contexts is fairly well documented, and some of the distances to source appear to be as extensive as other stone raw materials typical of embedded procurement by mobile foragers with large procurement ranges (Boulanger et al. 2015; Ellis 2011; Hoard et al. 1992; Shackley 1990, 1996; Speth et al. 2013). It's presence in North American early hunter-gatherer sites is well documented including Anzick, the La Prele Mammoth site, New Mexico's Arch Lake, and many others (Bement 1999; Frison and Stanford 1982; Morrow 2016; Roper 1991; Zarzycka et al. 2019).

LABORATORY SAMPLING, ANALYSIS AND INSTRUMENTATION

All source and archaeological samples were analyzed whole. The results presented here are quantitative in that they are derived from "filtered" intensity values ratioed to the appropriate x-ray continuum regions through a least squares fitting formula rather than plotting the proportions of the net intensities in a ternary system (McCarthy and Schamber 1981; Schamber 1977). Or more essentially, these data through the analysis of international rock standards, allow for inter-instrument comparison with a predictable degree of certainty (Hampel 1984; Shackley 2011).

The issue of accuracy using fundamental parameter calibrations of obsidian and in this case iron oxides with EDXRF for whole rock non-destructive analyses has been discussed elsewhere (http://swxrflab.net/anlysis.htm; Baxter 1994). Variability can be as great as one

percent, sometimes too great for source discrimination using non-destructive fundamental parameter analysis with EDXRF (see Brown and Nash 2014). Nevertheless, XRF has been found to be precise enough at the parts per million level in the analysis of non-volcanic rock for confident source assignment (see Moyo et al. 2016; c.f. Zarzycka et al. 2019).

Trace Element Analyses

All analyses for this study were conducted on a ThermoScientific *Quant'X* EDXRF laboratory spectrometer, located in the Geoarchaeological XRF Laboratory, Albuquerque, New Mexico, equipped with a thermoelectrically Peltier cooled solid-state Si(Li) X-ray detector, with a 50 kV, 50W, ultra-high-flux end window bremsstrahlung Rh target X-ray tube and a 76 µm (3 mil) beryllium (Be) window (air cooled), that runs on a power supply operating 4-50 kV/0.02-1.0 mA at 0.02 increments. The spectrometer is equipped with a 200 l min^{-1} Edwards vacuum pump, allowing for the analysis of lower-atomic-weight elements between sodium (Na) and titanium (Ti). Data acquisition is accomplished with a pulse processor and an analogue-to-digital converter. Elemental composition is identified with digital filter background removal, least squares empirical peak deconvolution, gross peak intensities and net peak intensities above background.

For the analysis of mid-Z condition elements Ti-Nb the x-ray tube is operated at 30 kV, using a 0.05 mm (medium) Pd primary beam filter in an air path at 100 seconds livetime to generate x-ray intensity $K\alpha_1$-line data for elements titanium (Ti), manganese (Mn), iron (as $Fe_2O_3^T$), cobalt (Co), nickel (Ni), copper, (Cu), zinc, (Zn), gallium (Ga), rubidium (Rb), strontium (Sr), yttrium (Y), zirconium (Zr), niobium (Nb), and $L\alpha_1$-line data for lead (Pb), and thorium (Th). Not all these elements are reported since their values in many rocks are very low and often outside the detection limits (see http://swxrflab.net/detectionlimits.htm). Trace element intensities were converted to concentration estimates by employing a linear or quadratic calibration line ratioed to the Compton scatter established for each element from the analysis of international rock standards certified by the National Institute of Standards and Technology (NIST), the US.

Geological Survey (USGS), Canadian Centre for Mineral and Energy Technology, and the Centre de Recherches Pétrographiques et Géochimiques in France, and the Japan Geological Survey (Govindaraju 1994). Line fitting is linear (XML) for all elements. When barium (Ba) is analyzed in the High Zb condition, the Rh tube is operated at 50 kV and up to 1.0 mA, ratioed to the bremsstrahlung region (see Davis 2011; Shackley 2011). Further details concerning the petrological choice of these elements in Southwest obsidians and other volcanic rocks is available in Shackley (1988, 1995, 2005, 2011; also Mahood and Stimac 1991; and Hughes and Smith 1993). Nineteen specific pressed powder standards are used for the best fit regression calibration for elements Ti through Nb, Pb, Th, and Ba, include G-2 (basalt), AGV-2 (andesite), GSP-2 (granodiorite), SY-2 (syenite), BHVO-2 (hawaiite), STM-1 (syenite), QLO-1 (quartz latite), RGM-1 (obsidian), W-2 (diabase), BIR-1 (basalt), SDC-1 (mica schist), TLM-1 (tonalite), SCO-1 (shale), NOD-A-1 and NOD-P-1 (oceanic manganese) all US Geological Survey standards, NIST-278 (obsidian), U.S. National Institute of Standards and Technology, BE-N (basalt) from the Centre de Recherches Pétrographiques et Géochimiques in France, and JR-1 and JR-2 (obsidian) from the Geological Survey of Japan (Govindaraju 1994).

Major and Minor Oxide Analysis

Analysis of the major oxides of Na, Mg, Al, Si, P, K, Ca, Ti, V, Mn, and Fe is performed under the multiple conditions elucidated below. The fundamental parameter analysis (theoretical with standards), while not as accurate as destructive analyses (pressed powder and fusion disks) is usually within a percent or less of actual, based on the analysis of the USGS RGM-1 obsidian standard (Shackley 2011). The fundamental parameters (theoretical) method is run under conditions commensurate with the elements of interest and calibrated with ten USGS standards (RGM-1, rhyolite; AGV-2, andesite; BHVO-1, hawaiite; BIR-1, basalt; G-2, granite; GSP-2, granodiorite; BCR-2, basalt; W-2, diabase; QLO-1, quartz latite; STM-1, syenite), and one

Japanese Geological Survey rhyolite standard (JR-1). The oxides are normalized to the RGM-1 USGS recommended versus measured values.

Conditions of Fundamental Parameter Analysis[1]

Low Za (Na, Mg, Al, Si, P)

Voltage	6 kV	Current	Auto[2]
Livetime	100 seconds	Counts Limit	0
Filter	No Filter	Atmosphere	Vacuum
Maximum Energy	10 keV	Count Rate	Low

Mid Zb (K, Ca, Ti, V, Cr, Mn, Fe)

Voltage	32 kV	Current	Auto
Livetime	100 seconds	Counts Limit	0
Filter	Pd (0.06 mm)	Atmosphere	Vacuum
Maximum Energy	40 keV	Count Rate	Medium

High Zb (Sn, Sb, Ba, Ag, Cd)

Voltage	50 kV	Current	Auto
Livetime	100 seconds	Counts Limit	0
Filter	Cu (0.559 mm)	Atmosphere	Vacuum
Maximum Energy	40 keV	Count Rate	High

Low Zb (S, Cl, K, Ca)

Voltage	8 kV	Current	Auto
Livetime	100 seconds	Counts Limit	0
Filter	Cellulose (0.06 mm)	Atmosphere	Vacuum
Maximum Energy	10 keV	Count Rate	Low

[1] Multiple conditions designed to ameliorate peak overlap identified with digital filter background removal, least squares empirical peak deconvolution, gross peak intensities and net peak intensities above background.

[2] Current is set automatically based on the mass absorption coefficient.

The data from the WinTrace software were translated directly into Excel for Windows software for manipulation and on into SPSS ver. 27 and JMP 12.0.1 software for plotting. In

order to evaluate these quantitative determinations, machine data were compared to measurements of known standards during each run. RGM-1 a USGS rhyolite standard was analyzed during each sample run of ≤19 to check machine calibration (Table 1; see Govindaraju 1994).

DISCUSSION

As noted above a multivariate to bivariate statistical analysis was performed on the source and archeological data to determine whether the artifacts were potentially procured from one of the three iron mines located in the region, Lien, Chicago or Sunrise. Typically principal components analysis (PCA) that assumes multivariate normality is used to explain the variance-covariance structure of a set of variables through a few linear combinations in multivariate space (Johnson and Wichern 1998:458). The value in PCA for geological and archaeological materials is in identifying those variables (elements in this case) that are most operative in the data (see Baxter 1994; Shennan 1997). However, compositional data are rarely multivariate normal (Baxter 1989, 1991, 1992a, 1994). This means that severely non-normal data cells in the sum of squares of the cross-products matrix can be empty and the associations (components) can be skewed. One method to ameliorate this issue is by using additional non-parametric methods such as cluster analysis and graphical displays, in our case bivariate plots (see Aldenderfer 1982; Baxter 1992b). This was the analytical trajectory used in this analysis, and one that appears to derive a good agreement between statistical methods (see Tables 1 through 3 and Figures 1 through 5).

First, four elements (oxides) that appeared to exhibit the greatest variability between the two sources, and yielded values above the detection limits (i.e. Al, Si, Ca, Fe) were plotted, all against Al as the independent variable which appeared to exhibit the greatest variability between the two sources (Figure 1, see Table 1). Discrimination on these variables appeared to be good, except for Ca, and provided the basis for variable (element) selection for a refined principal components analysis (PCA; see Tables 2 and 3, and Figure 2). Yttrium (Y) appeared to both

exhibit high multivariate variability and was partially correlated with the oxides, but the utility in a non-parametric cluster analysis suggested that it did not, the same with Ca.

Principal Components Analysis

First, the iron oxide source and artifact data are so dominated by three oxides Al, Si, and Fe in relatively high proportions that trace element values were quite low, many below detection limits, as discussed above (see http://swxrflab.net/detectionlimits.htm). Indeed, even though the source and archaeological samples were technically iron oxides, the iron content in the three sources varied between 21% and 94% (see Table 1). In the analysis of the source rocks, it became apparent the greatest variability was in Al, Si, Fe (Table 1). Preliminary bivariate plots suggested that the trace elements were not very discriminating even though many values were above the detection limits. The principal components analysis aided in this regard (Tables 2 and 3 and Figure 2).

The component plots and Eignevalue table indicated that Al, Si, and Fe were highly correlated, Al with Si, and Fe, and Ca less so with Fe, the latter not indicating significant correlation in the biplots (Tables 2 and 3 and Figure 2). With regard to the contribution of Al, Si, and Fe in the principal components analysis the first two components comprised over 96% of the variability with relatively high eigenvalues as can be seen in the scree plot, not unexpected given the high concentrations of Al, Si, and Fe generally (Figure 2). The cluster analysis using the variables (elements) Al, Si, Fe indicated, as the PCA analysis inferred, that the provenance of the artifacts from the Beach Cache were approximately evenly distributed between the three sources; and Sunrise and Chicago, located relatively nearby are likely from the same geological source formation (Table 1 and Figure 5). One note here is that a few of the source samples were miss-classified statistically likely due to the inherent variability of source material (iron oxide) that is formed at relatively low temperatures (see Table 1 and Figure 3). No explanation is offered for

these discrepancies here. The non-parametric cluster analysis did infer the misclassification based on the elements included in the analysis, as was also evident in the bivariate plots (see Figure 3).

So, was there a significant correlation between the results of the parametric principal components and non-parametric cluster and bivariate analyses? The answer is most certainly (Figures 2, 4 and 5). As can be seen by the bivariate plots with 90% confidence ellipse overlays that there is a good correlation between all three analyses, particularly non-parametric cluster and bivariate, despite the low temperature origin of the rock.

It is safe to conclude, that statistically approximately one-half of the artifacts were procured from the Lien iron source and one-half from the Sunrise or Chicago iron sources. The only caveat in this inference is that there could be other iron sources with similar composition, although these two sources using XRF can be statistically discriminated on at least three oxides suggesting that given the relative regional proximity of the sources to this site and these results that the artifacts were likely procured from one of these three sources.

REFERENCES CITED

Aldenderfer, M.S. 1982, Methods of cluster validation for archaeology. *World Archaeology* 14:61-72.

Baxter, M.J. 1989, The multivariate analysis of compositional data in archaeology: a methodological note. *Archaeometry* 31:45-53.

Baxter, M.J. 1991, An empirical study of principal component and correspondence analysis of glass compositions. *Archaeometry* 33:29-41.

Baxter, M.J. 1992a, Archaeological uses of the biplot - a neglected technique? In Lock, G., and Moffet, J. (Eds.) *Computer Applications and Quantitative Methods in Archaeology*, pp. 141-148. BAR International Series 577, Oxford.

Baxter, M.J. 1992b, Statistical analysis of chemical compositional data and the comparision of analyses. *Archaeometry* 34:267-277.

Baxter, M.J. 1994, *Exploratory Multivariate Analysis in Archaeology*. Edinburgh University Press.

Bement, L. 1999, *Bison Hunting at Cooper Site: Where Lightning Bolts Drew Thundering Herds*. Norman, University of Oklahoma Press.

Boulanger, M.T., Briggs, B., O'Brien, M.J., Redmond, B.G., Glascock, M.D., Eren M.I. 2015, Neutron activation analysis of 12,900 year-old stone artifacts confirms 450-510+ km Clovis tool-stone acquisition at Paleo Crossing (33ME274), northeast Ohio, USA. *Journal of Archaeological Science* 53:550-558.

Brown, F.H., and B.P. Nash, 2014, Correlation: Volcanic ash, obsidian. In H. Holland and K. Turekian (Eds.), *Treatise on Geochemistry*. Elsevier, Amsterdam

Davis, K.D., T.L. Jackson, M.S. Shackley, T. Teague, and J.H. Hampel, 2011, Factors affecting the energy-dispersive x-ray fluorescence (EDXRF) analysis of archaeological obsidian. In M.S. Shackley (Ed.) *X-Ray Fluorescence Spectrometry (XRF) in Geoarchaeology*, pp. 45-64. New York, Springer.

Ellis, C. 2011, Measuring Paleoindian range mobility and land-use in the Great Lakes/Northeast. *Journal of Anthropological Archaeology* 30:385-401.

Frison, G.C., and Stanford, D.J. 1982, The Agate Basin Site: A Record of teh Paleoindian Occupation of the Northwestern High Plains. New York, Academic Press.

Govindaraju, K.,1994,1994 Compilation of Working Values and Sample Description for 383 Geostandards. *Geostandards Newsletter* 18 (special issue).

Hampel, Joachim H., 1984, Technical considerations in x-ray fluorescence analysis of obsidian. In R.E. Hughes (Ed.) *Obsidian Studies in the Great Basin*, pp. 21-25. Contributions of the University of California Archaeological Research Facility 45. Berkeley.

Hildreth, W.
1981 Gradients in Silicic Magma Chambers: Implications for Lithospheric Magmatism. *Journal of Geophysical Research* 86:10153-10192.

Hoard, R.J., Holen, S.R., Glascock, M.D., Neff, H., Elam, J.M. 1992, Neutron activation analysis of stone from the Chadron Formation and a Clovis site on the Great Plains. *Journal of Archaeological Science* 19:655-665.

Hughes, Richard E., and Robert L. Smith
1993 Archaeology, Geology, and Geochemistry in Obsidian Provenance Studies. *In Scale on Archaeological and Geoscientific Perspectives*, edited by J.K. Stein and A.R. Linse, pp. 79-91. Geological Society of America Special Paper 283.

Johnson, R.A., and Wichern, D.W. 1998, *Applied Multivariate Statistical Analysis, 4th edition*. New York: Prentice-Hall, Inc.

Mahood, Gail A., and James A. Stimac
1990 Trace-Element Partitioning in Pantellerites and Trachytes. *Geochemica et Cosmochimica Acta* 54:2257- 2276.

McCarthy, J.J., and F.H. Schamber
1981 Least-Squares Fit with Digital Filter: A Status Report. In *Energy Dispersive X-ray Spectrometry*, edited by K.F.J. Heinrich, D.E. Newbury, R.L. Myklebust, and C.E. Fiori, pp. 273-296. National Bureau of Standards Special Publication 604, Washington, D.C.

Morrow, J.E. 2016, Evidence of Paleoindian spirituality and ritual behavior: large thin bifaces and other sacred objects from Clovis and other Late Pleistocene-Early Holocene cultural contexts. Fayetville, *Arkansas Archaeological Survey 67*:18-65.

Moyo, S., Mphuti, D, Curkowska, E, Henshilwood, C.S., et al. 2016, Blombos Cave: Middle Stone Age ochre differentiation through FTIR, ICP-OES, EDXRF, and XRD. *Quaternary International* 404:20-29.

Roper, D.C. 1991, A comparison of contexts of red ocher use in Paleoindian and upper Paleolithic sites. *North American Archaeology* 12:289-301.

Schamber, F.H., 1977, A modification of the linear least-squares fitting method which provides continuum suppression. In T.G. Dzubay (Ed.) *X-ray Fluorescence Analysis of Environmental Samples*, pp. 241-257. Ann Arbor Science Publishers.

Shackley, M. S., 1988, Sources of archaeological obsidian in the Southwest: an archaeological, petrological, and geochemical study. *American Antiquity* 53(4):752-772.

Shackley, M.S. 1990, *Early Hunter-Gatherer Procurement Ranges in the Southwest: Evidence from Obsidian Geochemistry and Lithic Technology*. Ph.D. dissertation, Department of Anthropology, Arizona State University, Tempe.

Shackley, M.S., 1995, Sources of archaeological obsidian in the greater American Southwest: an update and quantitative analysis. *American Antiquity* 60(3):531-551.

Shackley, M.S. 1996, Range and mobility in the early hunter-gatherer Southwest. In Roth, B. (Ed.) *Early Formative Adaptations in the Southern Southwest*, pp. 5-16. Monographs in World Prehistory 25. Prehistory Press, Madison.

Shackley, M.S., 2005, *Obsidian: Geology and Archaeology in the North American Southwest*. University of Arizona Press, Tucson.

Shackley, M.S. 2011, An introduction to x-ray fluorescence (XRF) analysis in archaeology. In M.S. Shackley (Ed.), *X-Ray Fluorescence Spectrometry (XRF) in Geoarchaeology*, pp. 7-44. Springer, New York.

Shennan, S. 1997, *Quantifying Archaeology, 2nd edition*. Iowa City, University of Iowa Press.

Speth, J.D., Newlander, K., White, A., Lemke, A.K., and Anderson, L. 2013, Paleoindian big-game hunting in North America: provisioning or politics. Quaternary International 285:111-139.

Zarzycka, S.E., Surovell, T.A., Mackie, M.E., Pelton, S.R., Kelly, R.L., Goldberg, P., Dewey, J., and Kent, M. 2019, Long-distance transport of red ocher by Clovis foragers. *Journal of Archaeological Science: Reports* 25:519-529.

Table 1. Major, and minor oxides, and selected trace element concentrations for the artifacts, and the USGS RGM-1 obsidian standard with recommended values.

Source/Sample	Sample	Source/character	Na2O	MgO	Al2O3	SiO2	P2O5	K2O	CaO	TiO2	V2O5	MnO	Fe2O3	Ni	Y	Nb	Pb
Sunrise	1	Sunrise	0.3	2.2	3.1	8.6	0.2	0.2	3.3	0.0	0.0	0.01	81.9	106	4	47	11
Sunrise	2	Sunrise	0.2	0.8	3.3	17.3	0.0	0.3	0.5	0.0	0.0	0.01	77.6	99	4	25	20
Sunrise	3	Sunrise	1.1	1.5	8.9	43.8	0.0	3.4	2.3	0.2	0.0	0.02	38.4	63	23	6	94
Sunrise	4	Sunrise	1.4	2.1	6.0	19.8	1.4	1.2	36.8	0.2	0.0	0.21	30.4	44	11	9	24
Sunrise	5	Sunrise	1.0	2.8	6.0	20.8	0.2	0.7	5.2	0.0	0.0	0.03	63.2	81	4	66	32
Sunrise	6	Sunrise	0.3	0.6	4.1	7.9	0.0	0.4	0.4	0.0	0.1	0.00	86.3	127	4	68	3
Sunrise	7	Sunrise	0.2	1.3	4.8	12.7	0.0	0.3	0.8	0.0	0.0	0.00	79.9	170	4	23	2
Sunrise	8	Sunrise	0.4	1.4	5.9	16.1	0.1	0.6	0.6	0.0	0.1	0.02	74.8	76	20	125	8
Sunrise	9	Sunrise	0.4	1.2	3.5	12.5	0.1	0.3	2.2	0.0	0.0	0.38	78.9	418	4	53	121
Sunrise	10	Sunrise	0.7	2.6	5.9	17.5	0.3	0.5	5.1	0.0	0.0	0.01	67.3	130	4	39	0
Sunrise	11	Sunrise	0.0	0.5	2.1	4.9	0.0	0.1	0.2	0.0	0.0	0.00	92.0	235	4	61	26
Sunrise	12	Sunrise	0.4	2.2	4.5	14.4	0.3	0.3	7.5	0.0	0.0	0.00	70.4	102	4	67	2
Sunrise	13	Sunrise	0.6	1.3	5.5	13.7	0.1	0.4	0.4	0.0	0.0	0.03	77.9	160	4	7	11
Lien	1	Lien	0.5	1.4	22.4	27.0	0.0	1.2	1.2	0.1	0.1	0.10	45.7	121	13	1	2
Lien	2	Lien	0.8	3.0	12.1	21.0	1.1	1.2	6.1	0.0	0.0	0.15	54.4	58	82	7	20
Lien	3	Lien	0.8	3.1	11.1	42.3	0.3	0.8	4.6	0.1	0.0	0.09	36.7	56	55	1	0
Lien	4	Lien	0.9	2.9	17.1	53.1	0.0	4.8	0.7	0.6	0.1	0.02	19.5	38	25	16	6
Lien	5	Lien	0.8	2.4	11.8	38.0	0.2	1.7	9.6	0.0	0.0	0.17	35.3	36	15	1	0
Lien	6	Lien	0.8	3.1	14.0	38.5	0.1	1.8	5.2	0.2	0.0	0.08	36.1	89	26	8	9
Lien	7	Lien	0.6	3.8	13.7	41.0	0.0	3.4	1.0	0.7	0.1	0.06	35.4	39	11	10	2
Lien	8	Lien	0.8	3.0	16.2	42.2	0.0	1.5	2.9	2.2	0.1	0.22	30.9	153	102	7	0
Lien	9	Lien	0.8	2.1	14.5	39.5	0.0	1.0	1.5	0.5	0.0	0.10	39.9	51	26	4	0
Lien	10	Lien	0.6	4.5	15.8	32.1	0.0	3.3	0.9	0.6	0.0	0.06	41.9	37	15	1	2
Chicago	C1	Chicago	1.3	14.5	0.9	2.1	0.7	0.2	12.9	0.0	0.0	0.1	66.8	415	6	2	149
Chicago	C2	Chicago	0.9	3.1	8.5	23.7	0.0	3.7	3.2	0.3	0.0	0.1	56.1	124	23	10	101
Chicago	C3	Chicago	0.1	0.7	0.5	1.1	0.0	0.1	0.9	0.0	0.1	0.0	96.2	150	4	1	-1
Chicago	C4	Chicago	1.1	1.5	19.4	48.9	0.0	6.2	1.0	0.5	0.0	0.0	21.1	79	19	11	50
Chicago	C5	Chicago	0.4	1.7	2.3	7.3	0.1	0.3	1.3	0.0	0.0	0.0	86.5	87	6	1	30
Chicago	C6	Chicago	0.4	2.5	3.4	8.0	0.1	0.3	2.3	0.0	0.0	0.0	82.8	338	4	3	122
Chicago	C7	Chicago	0.9	2.4	21.7	43.7	0.0	6.4	2.9	0.3	0.0	0.0	21.2	132	25	5	60
Chicago	C8	Chicago	0.3	1.0	3.4	10.2	0.0	0.7	0.9	0.0	0.1	0.1	83.2	253	6	15	34
Chicago	C9	Chicago	0.2	1.1	0.8	2.0	0.1	0.2	1.0	0.0	0.0	0.0	94.4	109	4	21	18

Source/Sample	Sample	Source/character	Na2O	MgO	Al2O3	SiO2	P2O5	K2O	CaO	TiO2	V2O5	MnO	Fe2O3	Ni	Y	Nb	Pb
Chicago	C10	Chicago	1.6	0.3	2.1	9.2	0.2	3.1	2.1	0.0	0.0	0.1	81.1	123	4	4	56
13-11	13-11	earthy	1.4	0.0	8.9	15.7	0.3	0.2	0.9	2.7	0.1	0.2	67.6	33	116	95	20
13-62	13-62	earthy	3.6	0.0	8.0	17.6	0.7	0.1	4.9	3.0	0.1	0.2	61.6	20	70	21	10
13-77	13-77	earthy	2.6	0.1	10.3	36.2	0.4	0.6	2.4	2.8	0.1	0.1	42.7	20	35	27	10
13-86	13-86	earthy	0.6	0.0	19.6	37.3	0.0	0.1	0.6	7.0	0.1	0.1	34.0	20	58	95	12
14-7	14-7	earthy	2.8	0.2	10.5	31.0	0.6	0.2	2.1	4.4	0.2	0.2	45.6	26	23	38	8
14-45	14-45	earthy	4.2	0.1	4.4	14.4	2.1	0.2	46.3	3.9	0.1	0.1	23.2	17	27	26	7
14-54	14-54	earthy	3.1	0.2	8.9	27.5	0.7	0.5	7.6	1.6	0.1	0.5	47.8	36	49	9	8
17-23	17-23	earthy	0.7	0.0	22.9	35.6	0.1	0.1	0.9	3.5	0.1	0.2	34.5	30	29	59	5
14-31	14-31	rocky	1.4	0.5	1.7	7.4	0.3	0.4	0.5	0.0	0.0	1.0	85.9	21	4	3	0
14-71	14-71	rocky	0.5	1.5	3.3	11.1	0.2	0.5	0.8	0.0	0.0	1.8	79.4	38	10	6	0
14-101	14-101	rocky	1.5	0.6	2.7	11.8	0.3	0.6	0.8	0.0	0.0	3.0	77.7	106	7	1	0
14-116	14-116	rocky	2.4	0.5	1.9	8.2	0.4	0.6	1.1	0.0	0.0	1.5	82.6	67	13	7	0
14-123	14-123	rocky	1.2	2.2	4.7	16.6	0.6	0.5	11.9	0.0	0.0	5.0	56.6	52	15	1	0
14-168	14-168	rocky	1.7	0.5	2.7	12.4	0.3	0.7	1.6	0.0	0.0	1.3	78.0	43	25	1	0
14-186	14-186	earthy	1.7	0.5	3.0	15.4	0.3	0.7	1.2	0.0	0.1	0.7	75.9	31	22	5	3
14-194	14-194	earthy	2.7	0.0	9.1	17.5	0.5	0.1	1.1	6.0	0.2	0.2	61.7	22	55	107	18
14-222	14-222	rocky	2.0	0.2	2.2	9.9	0.4	0.8	2.1	0.0	0.1	1.2	80.0	32	18	1	7
14-234	14-234	rocky	2.3	0.7	1.3	6.5	1.4	0.4	29.9	0.0	0.0	1.3	55.7	28	39	2	0
14-288	14-288	rocky	1.6	0.7	3.2	13.6	0.3	0.7	0.9	0.0	0.1	1.1	76.8	32	30	5	0
14-352	14-352	rocky	1.7	0.6	2.2	8.5	0.4	0.5	0.8	0.0	0.0	2.1	82.0	112	15	1	78
18-3	18-3	earthy	0.8	0.0	20.9	37.5	0.0	0.1	2.1	4.4	0.1	0.1	33.1	25	33	52	8
RGM-1			4.14	0.00	12.92	73.77	0.00	4.94	1.43	0.29	0.02	0.04	2.22	16	26	11	19
RGM-1 recommended			4.07	0.28	13.70	73.40	nr	4.30	1.15	0.27	nr	0.04	1.86	nr	25	9	24

Table 2. Component Eigenvalues of those values for Na, Mg, Al, Ca, Ti, Fe, Ni. Note that the first two components comprise only about 73% of the variability within the data, but Al, Si, and Fe exhibit the highest values in the first component.

Element	Prin1	Prin2	Prin3	Prin4
Na2O	0.03416	-0.43697	-0.20145	0.37316
MgO	0.16953	0.45886	-0.16113	-0.03671
Al2O3	**0.43798**	0.06502	0.18682	-0.12692
SiO2	**0.45046**	0.17049	0.08251	0.07617
K2O	0.26096	0.38463	-0.13331	0.20541
CaO	0.03832	-0.18107	-0.26862	0.43977
TiO2	0.25124	-0.40078	0.29275	0.01472
MnO	-0.18285	-0.08517	-0.38447	-0.01879
Fe2O3	**-0.46183**	-0.01109	0.03973	-0.24801
As2O5	-0.22271	0.13559	0.26014	0.48622
Ni	-0.25349	0.27963	0.29423	0.03618
Y	0.23925	-0.24725	0.14376	0.0652
Nb	-0.02348	-0.17866	0.51724	-0.18703
Pb	-0.15586	0.16385	0.35253	0.51271

Table 3. Eigenvectors for the selected elements Al, Si, Ca, Fe (variables) of the first four principal components and cumulative percentages of those components (see Scree Plot, Figure 3). Selection of these elements increases the proportion of variability from less than 73% for the 7 elements (see Table 2) to over 96% with the selection of Al, Si, Fe, and Y here indicating that much of the correlation in the data are contained in these four elements particularly the oxides of Al, Si, and Fe. This is similarly reflected in the cluster analysis groups and the bivariate plots (see Figures 4 and 5). While Al, Si, and Fe are included in the first principal component, Ca was not.

	Prin1	**Prin2**	**Prin3**	**Prin4**
Al2O3	0.56823	-0.19252	0.76818	0.22351
SiO2	0.58447	-0.12976	-0.61438	0.51390
CaO	0.02925	0.93358	0.11383	0.33856
Fe2O3	-0.57850	-0.27301	0.13957	0.75586

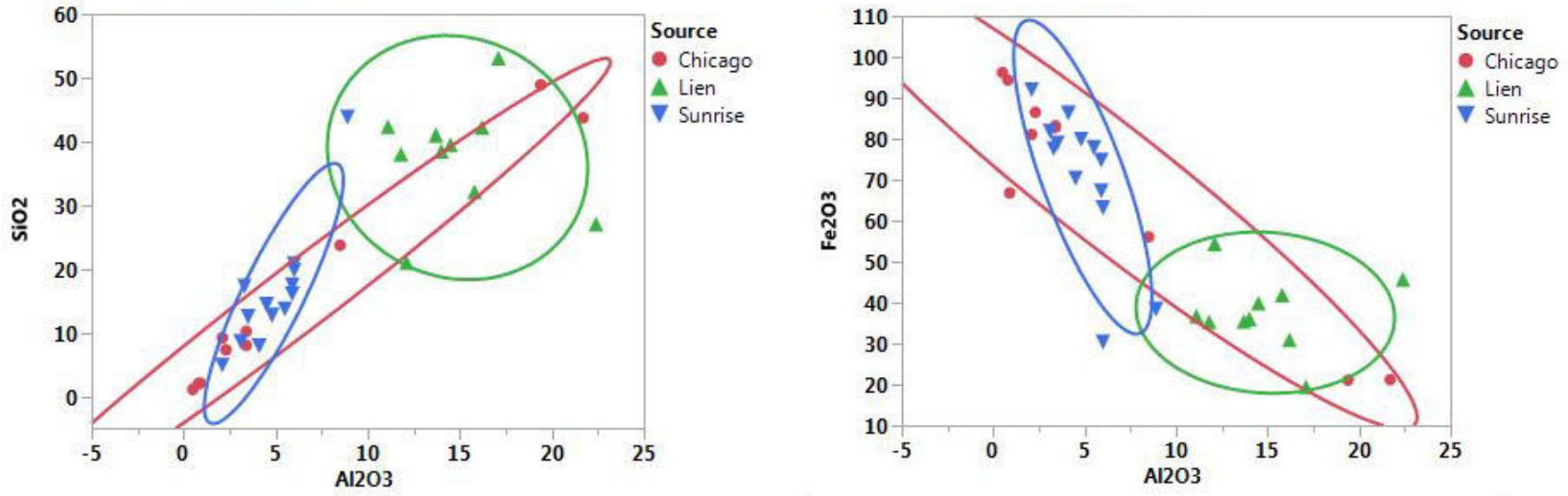

Figure 1. Al/Si (left), and Al/Fe (right) bivariate plots of the Lien, Sunrise and Chicago source rocks indicating significant discrimination on those three oxides and elements. Confidence ellipses at 90%. Note the two Chicago samples misclassified as in the cluster analysis on Fe (Figure 3, see text).

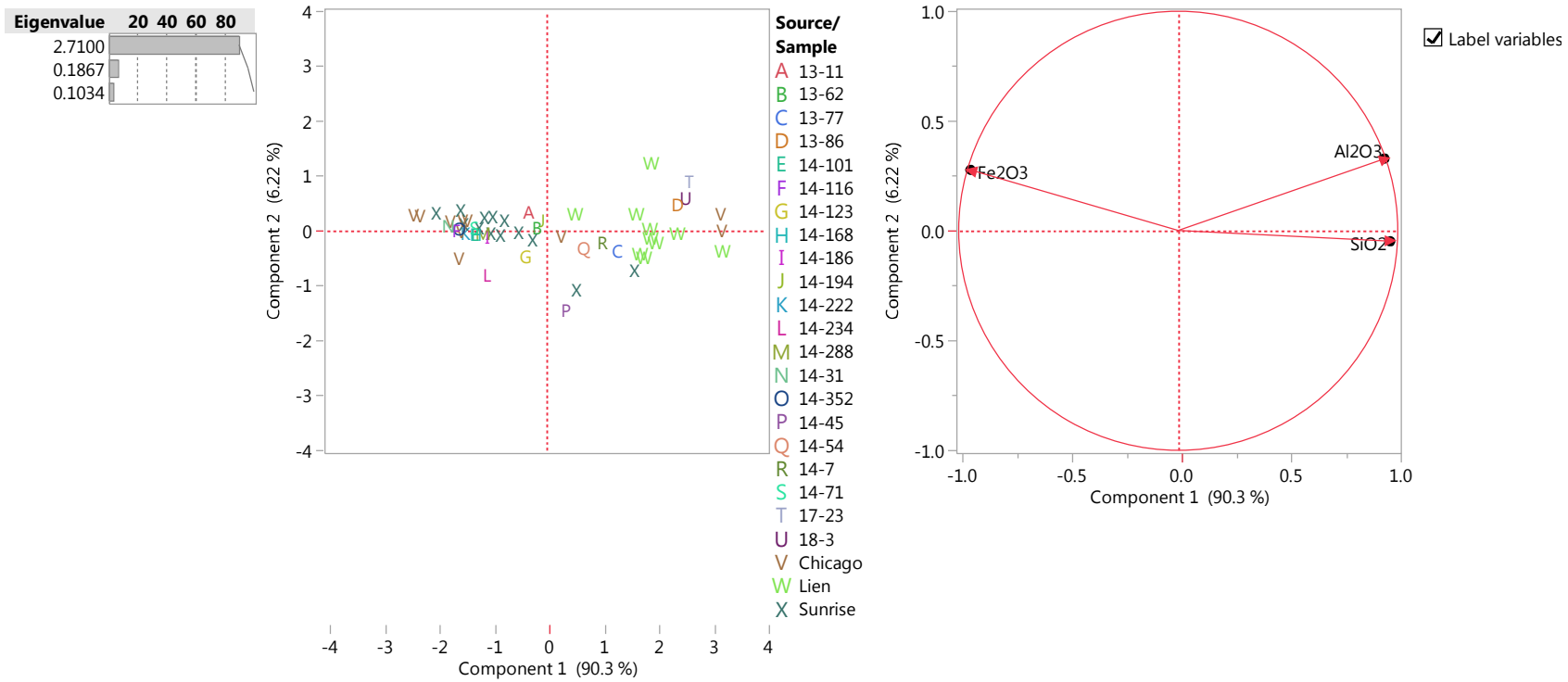

Figure 2. PCA score plot (left) and loading plot (right) for the three selected elements. Note how correlated Al and Si are in this analysis.

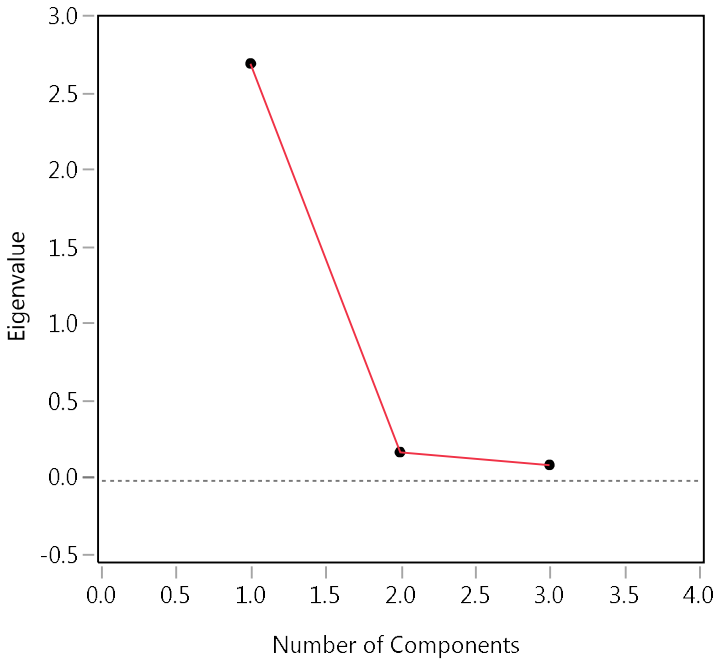

Figure 3. Scree plot of the Eigenvalues versus principal components for the three selected elements. Note that the first two components occur just before the curve indicating that the majority of variability is contained in those two components in this case over 96% "above the elbow" (Johnson and Wichern 1994:475).

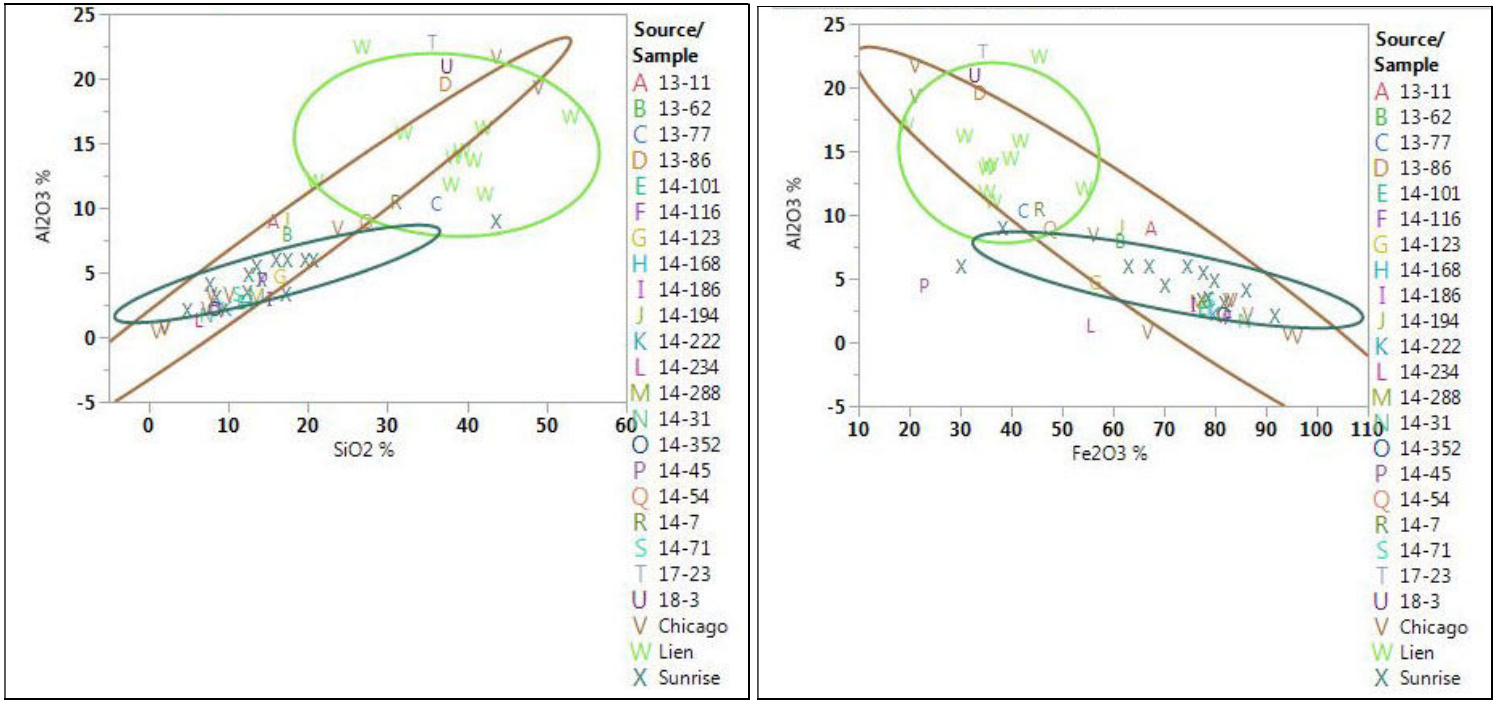

Figure 4. Al/Si (tleft); Al/Fe (right) bivariate plots of Lien, Sunrise and Chicago source rocks, and the Beach Cache artifacts by sample number. Compare to the groupings in the cluster analysis (Figure 3). Confidence ellipses at 90%. Parenthetically, note that Beach Cache samples 13-11, 13-62, and 14-194 plot nearly on top of each other here and in the cluster analysis, and their data are quite similar, even more so with most of the rocky artifacts (see Table 1). It is possible that these are fragments of the same rock, given EDXRF precision.

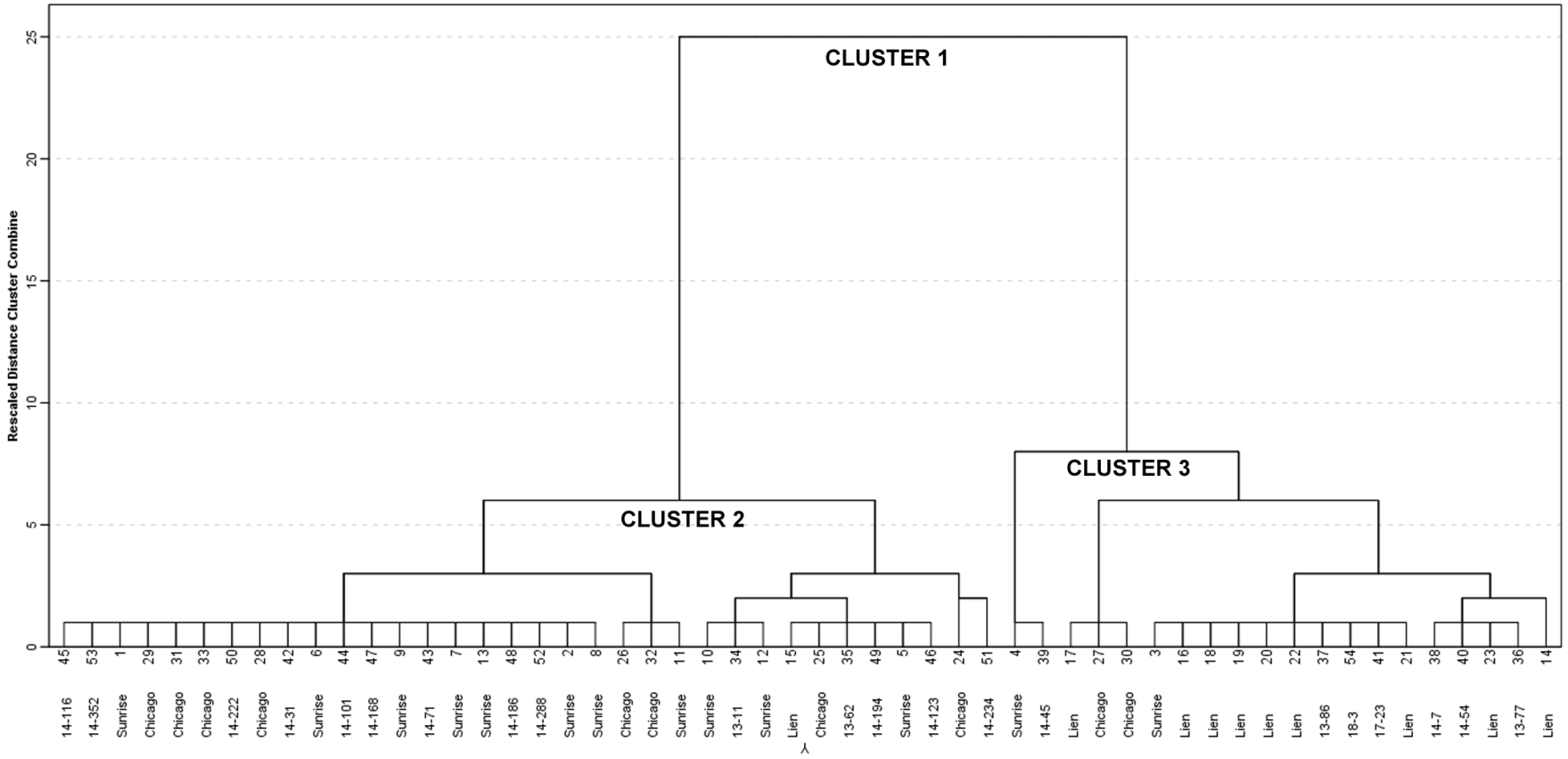

Figure 5. Average linking (between groups) method, squared Euclidean distance cluster dendrogram of the Lien, Sunrise, and Chicago source data and the Beach Cache artifacts by sample number (four clusters were assumed as priors). Elements used in the analysis include Al, Si, Fe as in the bivariate plots. There are some misclassifications (i.e. Chicago 27 and 30 are the only Chicago source rocks within the Lien source cluster) also reflected in the bivariate plots (Figure 4).